Available online at www.sciencedirect.com
SCIENCE DIRECT®
Journal of Solid State Chemistry 179 (2006) 613–622
JOURNAL OF SOLID STATE CHEMISTRY
www.elsevier.com/locate/jssc

Lanthanide distribution in some doped alkaline earth aluminates and gallates

Paul J. Saines[a], Margaret M. Elcombe[b], Brendan J. Kennedy[a,*]

[a]School of Chemistry, The University of Sydney, Sydney, NSW 2006, Australia
[b]Bragg Institute, Australian Nuclear Science and Technology Organisation, Lucas Heights, NSW, 2234, Australia

Received 9 August 2005; received in revised form 26 October 2005; accepted 28 October 2005
Available online 4 January 2006

Abstract

High-resolution neutron and synchrotron X-ray powder diffraction studies are reported for the six oxides AB_2O_4 ($A = Ca^{2+}$, Sr^{2+} and Ba^{2+} and $B = Al^{3+}$ and Ga^{3+}). These oxides all adopt a stuffed tridymite type structure, the precise nature of which depends on both the *A*- and *B*-type cations. Bond valence calculations reveal a range of values for the various *A*-type cations, in all cases at least one site is significantly underbonded. Conversely the tetrahedral *B*-type sites invariably exhibit unexceptional bond valencies. Attempts to dope the oxides with various lanthanides to the 1% level invariably resulted in some segregation into alternate phases located at the grain boundaries. The identity of the impurity phases is presented and the importance of bond valencies in understanding this segregation is highlighted.

Keywords: Alkaline earth; Aluminates; Gallates; Neutron diffraction; X-ray diffraction; Lanthanides; Stuffed tridymites

1. Introduction

Persistent luminescent materials are a ubiquitous part of everyday life, finding use in a wide range of commercial applications such as luminescent watch dials and emergency lighting [1,2]. Europium (II) doped alkaline earth aluminates (AAl_2O_4:Eu^{2+}) have several advantages over the traditionally used sulphide-based phosphors including their lack of radioactive elements and their lower chemical toxicity. They have also been described as offering higher chemical and moisture stability compared to the sulphide phosphors [1,3]. These oxides have been further developed by the incorporation of Ln^{3+} co-activators, most commonly neodymium and dysprosium [2]. These co-activators result in a more than 10-fold increase in the initial intensity of luminescence and an afterglow described as being "easily visible", with the naked eye, for over 10 h after exposure to illumination [1]. The colour and lifetime of the luminescence is dependant on the alkaline earth cation (*A*) with the strontium compound $SrAl_2O_4$ showing the most promise. Establishing the precise structures of the alkaline earth aluminates is crucial to understanding their properties and in particular how differences in the structure of these alkaline earth aluminates influences properties such as the solubility of the co-activating Ln^{3+} ions and the varying effectiveness of the various Ln^{3+} co-activator ions.

The alkaline earth aluminates, and the structurally analogous gallates, have the empirical formula AB_2O_4 where A^{2+} is the divalent cation (Ca^{2+}, Sr^{2+} and Ba^{2+}) and B^{3+} is the trivalent cation (Al^{3+} or Ga^{3+}). These compounds adopt a stuffed tridymite-type structure. The tridymite structure consists of corner sharing SiO_4 tetrahedra which connect together to form six-membered rings. In the stuffed tridymite structure the large divalent cation occupies the centre of the rings of AlO_4 or GaO_4 tetrahedra.

In the stuffed tridymite structure a compromise must be made between the bonding requirements of the A^{2+} ions and the B^{3+} ions. This can be seen in the distortion of the B_2O_4 framework particularly for the alkaline earth gallates and $CaAl_2O_4$ where a range of ring sizes form [4–12].

*Corresponding author. Fax: +61 2 9351 3329.

0022-4596/$ - see front matter © 2005 Published by Elsevier Inc.
doi:10.1016/j.jssc.2005.10.043

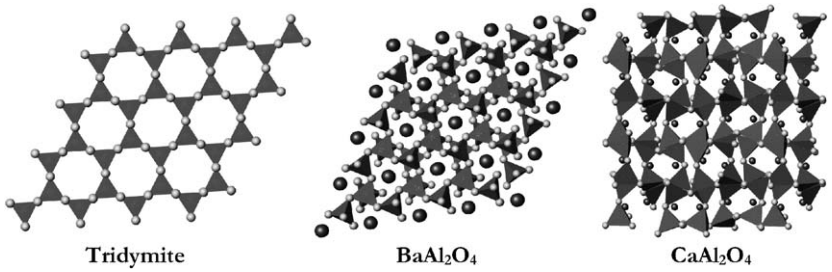

Fig. 1. A comparison of the *a–b* planes of tridymite, $BaAl_2O_4$ and $CaAl_2O_4$. The silicon and aluminium ions sit in the centre of the tetrahedra with the spheres representing the oxygen ligands. In the aluminates the spheres in the channels are the alkaline earth cations.

Additionally the co-ordination number of the alkaline earth ion sites varies across the six compounds presumably as a consequence of the differences in the size of the A-type cation [4–12] (Fig. 1).

This paper presents a systematic study of the structures of the alkaline earth aluminates and gallates using a combination of synchrotron X-ray and neutron powder diffraction. The refined structures are then used to rationalise the distribution of Eu^{2+} and Ln^{3+} ions within the various alkaline earth ion sites in these compounds. Finally the solubility of Eu^{2+}, Eu^{3+} and Nd^{3+} in these six host structures is determined qualitatively using a combination of X-ray diffraction (XRD), scanning electron microscopy (SEM), energy dispersive X-ray (EDX) analysis and electronic spectroscopy.

Table 1
Total heating times and temperatures required for the synthesis of samples of each of the six alkaline earth aluminates and gallates

Sample	Small sample		Large sample	
	Total time (h)	Temperature (°C)	Total time (h)	Temperature (°C)
$CaAl_2O_4$	96	1250	72	1250
$SrAl_2O_4$	60	1150	20	1150
			24	1250
$BaAl_2O_4$	60	1150	20	1150
$CaGa_2O_4$	96	1250	72	1250
$SrGa_2O_4$	96	1250	72	1250
$BaGa_2O_4$	40	1150	None	None

2. Synthesis and characterisation

Starting materials used were Ln_2O_3 (Ln = Eu or Nd) (Aldrich, 99.9%), ACO_3 (A = Ca, Sr or Ba) (Aldrich 99.9+ %), Al_2O_3 (Engis Australia 99.9%) and Ga_2O_3 (Aldrich 99.99+ %) with the Ln_2O_3 being dried by heating at 1000 °C prior to use. Samples were prepared from stoichiometric amounts of the appropriate starting materials. The samples were finely ground and heated in a muffle furnace for 16 h at 850 °C. After this the samples were heated as per the conditions listed in Table 1. The small samples refer to the synthesis of approximately 4 g samples and the conditions listed for the large samples refer to the additional heating required for 20 g samples compared to the smaller samples. Heating was usually carried out in intervals of 20 or 24 h with the samples being reground after each heating period.

A total of 4 g samples of 1 mol% Eu^{3+} and Nd^{3+} doped alkaline earth aluminates and gallates were prepared from finely ground stoichiometric mixtures of the appropriate alkaline earth carbonates, the appropriate rare earth oxide and aluminium or gallium oxide such that the samples had the stoichiometry $A_{0.99}Ln_{0.01}B_2O_4$, which hereafter are referred to as $A_{0.99}B_2O_4$:Ln^{3+} 1%. These samples were heated according to the same schedule used for the corresponding undoped compounds. With the exception of the calcium gallate samples, the various doped samples were ultimately heated for 24 h at a temperature 100 °C higher than the highest temperature used to prepare the smaller sized samples of the undoped compounds, to ensure the reaction had reached completion. The calcium gallate samples were fired for two additional periods of 48 h at 1250 °C, the highest temperature used to synthesise calcium gallate. A significantly higher temperature could not be used as it results in melting of the sample.

Two approaches were taken in an attempt to obtain reduced europium doped samples. The first of these involved the preparation of approximately 1 g samples of 1 mol% europium doped strontium and barium aluminates from finely ground stoichiometric mixtures of the appropriate alkaline earth carbonate, aluminium oxide and europium oxide. The mixtures were heated under a reducing atmosphere of 20% H_2/80% Ar. The europium doped alkaline earth aluminate compounds were initially heated at 850 °C for 16 h and, after regrinding, were then heated at 1150 °C for two periods of 20 h. $SrAl_2O_4$:Eu^{2+} 1% was then heated at 1000 °C for 72 h. Henceforth this method for preparing reduced samples will be known as the pre-cursor method.

The second synthetic route used to obtain Eu^{2+} was carried out via heating the previously synthesised Eu^{3+} doped alkaline earth-aluminates at 1000 °C. Samples were heated under a reducing atmosphere of 20% H_2/80% Ar and this method will be subsequently known as the pre-formed method. Approximately 1 g samples of Eu^{3+} doped calcium and strontium aluminate were heated for

26.5 days, while Eu^{3+} doped barium aluminate was heated for approximately 15.5 days. Approximately 1 g of the Eu^{3+} doped calcium aluminate was heated for approximately 27 days.

$CaEuAl_3O_7$ and $CaNdAl_3O_7$ were synthesised using a modification of methods described in the literature [13,14] with a mixture of the appropriate starting material being heated for 30 h at 1350 °C followed by up to three periods of 24 h at 1450 °C.

$EuAlO_3$ was synthesised following a method similar to that employed by Kanke and Navrotsky [15]. Stoichiometric quantities of europium carbonate and aluminium oxide were finely ground and the resulting mixture heated at 1250 °C for 24 h, 1350 °C for 24 h, 1450 °C for 24 h and finally 1550 °C for two periods of 48 h. $NdAlO_3$ was prepared using $Al(NO_3)_3 \cdot 9H_2O$ (Aldrich 99.9%) instead of Al_2O_3 with stoichiometric quantities of $Al(NO_3)_3 \cdot 9H_2O$ and Nd_2O_3 being heated for 20 h at 600 °C, 24 h at 800 °C and finally 120 and 240 h at 1200 °C. The compounds formed were characterised by powder XRD.

The phase purity of the samples was examined using a Shimadzu Lab X-6000 Diffractometer (40.0 kV, 30.0 mA, divergence and scatter slits 1.0° and receiver slit 0.6 mm) using Cu-K_α radiation using a scan rate of 1°/min. Subsequently these samples were also characterised by SEM, EDX analysis and electronic spectroscopy.

SEM and EDX analysis were conducted using sintered pellets produced by applying 5–6 t of pressure onto a 13 mm disc. The pellets were then heated at either 1100 °C for 16 h for the samples heated in air or 1000 °C for 48 h for the samples synthesised under a reducing atmosphere of 20% H_2/80% Ar. Analysis was carried out using either a Phillips XL 30 scanning electron microscope operating at 20 keV and a spot size setting of 5 or a Phillips 505 scanning electron microscope operating at 25 keV and a spot size of between 50 and 100 nm. The EDX analysis was performed using an EDAX model P-505 or XL-30 operated under the DX-4eDX ZAF operating system (Version 2.20 or 3.3). Analysis was performed using the propriety software in this system.

The electronic spectra of samples were measured using a Cary 5E UV-Vis-NIR spectrometer equipped with a diffuse reflectance attachment. Data were collected between 200 and 2800 nm, using a data interval of 0.667 nm and a scanning rate of 200 nm/min. $BaSO_4$ was used as the background for baseline scans.

Powder synchrotron XRD patterns were obtained at the Australian National Beamline Facility (ANBF) in Tsukba, Japan [16]. Data were obtained over the range of 5–125° (2θ angle) using up to three separate image plates as detectors employing X-rays at a wavelength of 0.8082 Å. The samples were housed in 0.3 mm capillaries that were rotated throughout the measurement. Powder neutron diffraction patterns were obtained using the HIGH-Resolution Powder Diffractometer (HRPD) at the High-Flux Australian Reactor (HIFAR) facility, Australian Nuclear Science and Technology Organisation (ANSTO), Lucas Heights Science and Technology Centre [17]. Samples of $SrAl_2O_4$, $BaAl_2O_4$, $CaGa_2O_4$ and $SrGa_2O_4$ were placed in 12 mm vanadium cylinders while samples of $CaAl_2O_4$ and $BaGa_2O_4$ were placed in 16 mm cylinders. Diffraction patterns were obtained at room temperature. A cryofurnace was used to obtain additional diffraction data of $BaAl_2O_4$ at 17 and 450 K. Data were collected using a wavelength of 1.884 Å from 5° to 150° (2θ angles) with a step size of 0.05° (2θ angle) (Fig. 2).

The Rietveld method was used to refine separate structures from both the powder X-ray and neutron diffraction data using the computer program Rietica [18]. For the first image plate data from the synchrotron a linear interpolation between regions were there were no Bragg peaks was used to fit the background. In all other cases a polynomial function was used to fit the background. In all cases a pseudo-Voight peak shape was employed using the Howard asymmetry correction where necessary [18].

Compound	Experimental			Literature		
	a (Å)	*b* (Å)	*c* (Å)	*a* (Å)	*b* (Å)	*c* (Å)
$NdAlO_3$	5.32167(7)	5.32167(7)	12.9239(2)	5.3223(2)	5.3223(2)	12.9292(5)
$EuAlO_3$	5.27163(5)	5.29257(4)	7.45990(7)	5.269(1)	5.291(1)	7.456(1)
$CaNdAl_3O_7$	7.7627(3)	7.7627(3)	5.1176(2)	7.7591(3)	7.76274(3)	5.1183(3)
$CaEuAl_3O_7$	7.72662(3)	7.72662(3)	5.08152(3)	7.7226(2)	7.7226(2)	5.0788(2)

3. Results

The diffraction patterns revealed that the samples of $SrAl_2O_4$, $BaAl_2O_4$, $SrGa_2O_4$ and $BaGa_2O_4$ were single phase. Although the small sample of $CaAl_2O_4$ was synthesised in pure form the larger sample, needed for neutron diffraction measurements, was found to contain an unidentified peak with an intensity approximately 0.4% of the largest peak of $CaAl_2O_4$ using conventional (laboratory) XRD. This additional peak was well below the background level in the neutron diffraction pattern. The samples of $CaGa_2O_4$ were found to contain a small amount of

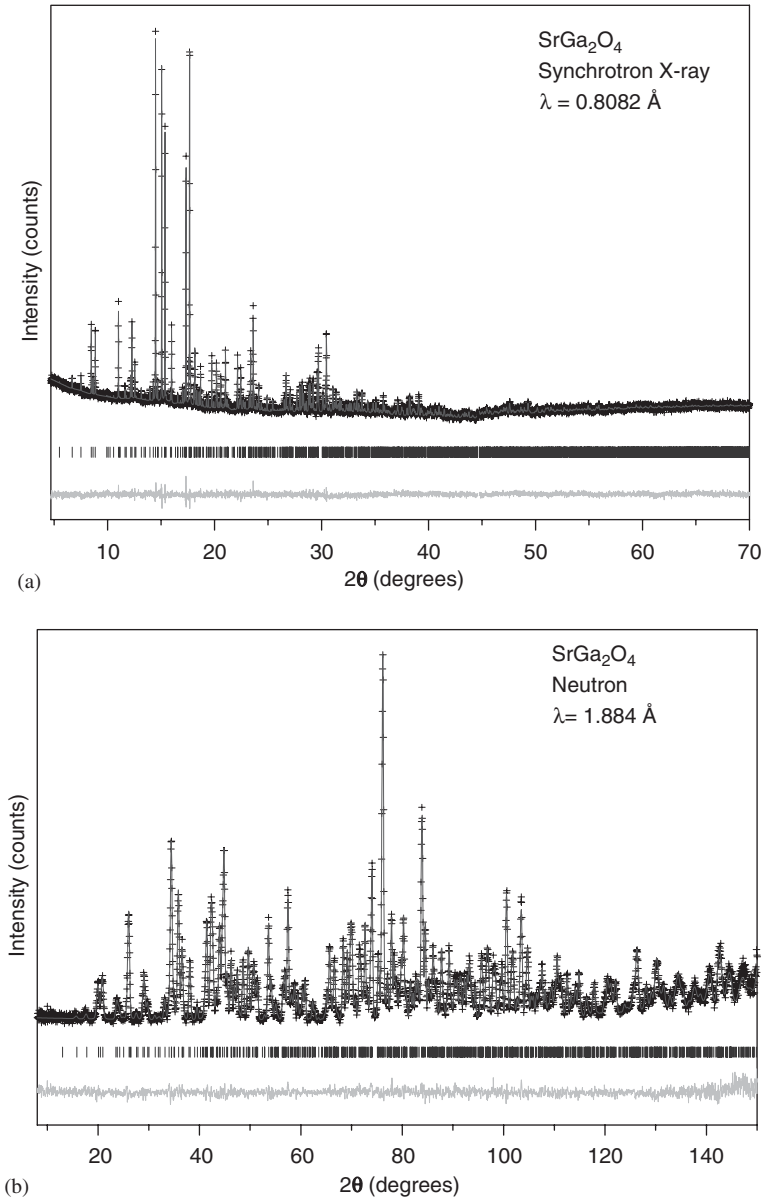

Fig. 2. Refined powder synchrotron X-ray (a) and neutron diffraction pattern (b) for $SrGa_2O_4$. The data is represented by the crosses and the calculated profile by the upper continuous line. The lower continuous line is the difference between the observed and calculated profiles. The vertical markers show the positions of the allowed Bragg reflections of $SrGa_2O_4$.

tricalcium tetragallium oxide ($Ca_3Ga_4O_9$) in addition to the desired product. The Rietveld refinement from the neutron data showed the sample contained 97.3 ± 0.8 mol% $CaGa_2O_4$ and 2.70 ± 0.09 mol% of $Ca_3Ga_4O_9$.

The XRD patterns of the Eu^{3+} and Nd^{3+} containing samples showed weak peaks, in addition to those present in the undoped samples, suggesting the formation of multiple phases. These additional, weak, peaks were identified as coming from various Eu^{3+} and Nd^{3+} containing phases, the actual species depending on both the Ln^{3+} and other cations. $EuAlO_3$ and $NdAlO_3$ formed in the doped strontium and barium aluminates. Samples of Eu^{3+} and Nd^{3+} doped calcium aluminate, calcium and strontium gallates and neodymium doped barium gallate contained $ALnM_3O_7$ (where $A^{2+} = Ca^{2+}$, Sr^{2+} or Ba^{2+}, $Ln^{3+} = Eu^{3+}$ or Nd^{3+} and $M^{3+} = Al^{3+}$ or Ga^{3+}). Europium doped barium gallate contained a peak belonging to an unidentified, presumably Eu^{3+} containing, phase. The segregation of these phases was confirmed using a combination of SEM and EDX analysis which indicated that the europium and neodymium segregated into separate grains generally at the boundaries between larger grains with no europium or neodymium being detected outside these regions. These results also showed that the unidentified phase in Eu^{3+} doped barium gallate was a europium enriched phase. In addition to these phases $Ca_{0.99}Ga_2O_4$:Ln^{3+} 1% was found to contain additional peaks corresponding to $CaGa_4O_7$. (Fig. 3)

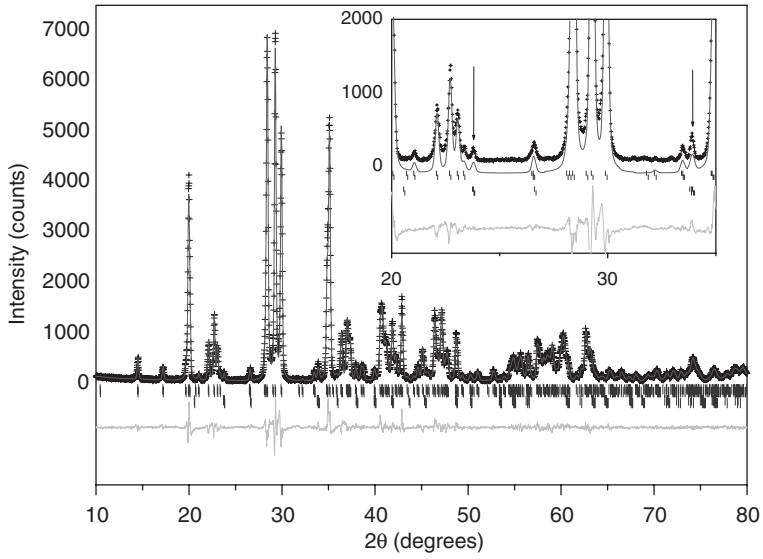

Fig. 3. Conventional X-ray diffraction pattern of $Sr_{0.99}Al_2O_4:Eu^{3+}$ 1%. The upper band of Bragg reflections correspond to $SrAl_2O_4$ and the lower band to $EuAlO_3$. The two peaks indicated by the arrows correspond to the two most evident peaks of $EuAlO_3$. The format is the same as for Fig. 2.

The powder XRD patterns for the samples of europium doped alkaline earth aluminates, heated under reducing conditions, revealed significant differences compared to those of samples heated in air. Samples of $Sr_{0.99}Al_2O_4:Eu^{2+}$ 1% and $Ba_{0.99}Al_2O_4:Eu^{2+}$ 1% synthesised using the pre-cursor method did not contain any $EuAlO_3$. Similarly synthesising $Sr_{0.99}Al_2O_4:Eu^{2+}$ 1% and $Ba_{0.99}Al_2O_4:Eu^{2+}$ 1% via the pre-formed method resulted in the elimination of $EuAlO_3$ after heating for 19 and 15.5 days, respectively. $Ca_{0.99}Al_2O_4:Eu^{2+}$ 1% heated for 23 days following the pre-formed method still contained peaks corresponding to $CaEuAl_3O_7$ but with significantly decreased intensity. SEM and EDX analysis of reduced samples synthesised by both the pre-formed and pre-cursor routes revealed that the regions of europium and neodymium enrichment were significantly reduced, and in the majority of samples eliminated entirely, upon reduction indicating that the europium is more uniformly distributed in the reduced samples (Fig. 4).

4. Discussion

Synchrotron X-ray and neutron diffraction data was used to obtain accurate and precise structures for the alkaline earth aluminates and gallates. Synchrotron XRD data were used to confirm the space group of the phases and to obtain precise unit cell parameters. The diffraction patterns obtained were consistent with the space groups assigned previously to these compounds [4,5,8,10–12,19,20].

The neutron diffraction data was used to refine accurate oxygen positions in the structures. Ultimately this allowed more accurate bond distances and bond angles to be determined. This information was used to establish which sites the Ln^{3+} ions may occupy in the doped compounds. Excellent fits were obtained for calcium and strontium aluminate as well as calcium and strontium gallate as evident from Table 2.

The results obtained for barium aluminate highlights the benefits of using neutron diffraction, over XRD, even when using a synchrotron source. Although the fit to the synchrotron XRD data for barium aluminate appeared to be excellent, the difference neutron profile showed a number of problems in modelling the intensity of a number of peaks in the pattern (see Fig. 5b). Since an excellent fit was obtained for the XRD pattern, the most likely cause for the problem is related to the position of the oxygen ions. Abakumov et al. used high-resolution electron diffraction to examine weak super-lattice reflections and showed that barium aluminate undergoes a broad transition between 400 and 670 K from a $P6_3$ room temperature ferroelectric phase to a $P6_322$ high-temperature paraelectric phase [19]. The precise structure of the high-temperature phase has not been unequivocally established, with two different structures proposed [6,7,21]. The difference between the three structures relates to the positions of the oxygen ions.

Two approaches were taken in order to determine if the poorer fit of the model to the neutron data was related to partial trapping of the high-temperature phase at room temperature. The first involved collecting a neutron diffraction pattern at 450 K (the highest temperature accessible with the cryofurnace) in an attempt to characterise the paraelectric phase. Refinement of both the room temperature and the 450 K patterns were attempted using both high-temperature phases and a combination of a high-temperature and the low-temperature phase. None of these approaches resulted in any significant improvement in the fit in either of the patterns suggesting the presence of the high-temperature phase was not the cause of the poorer fit.

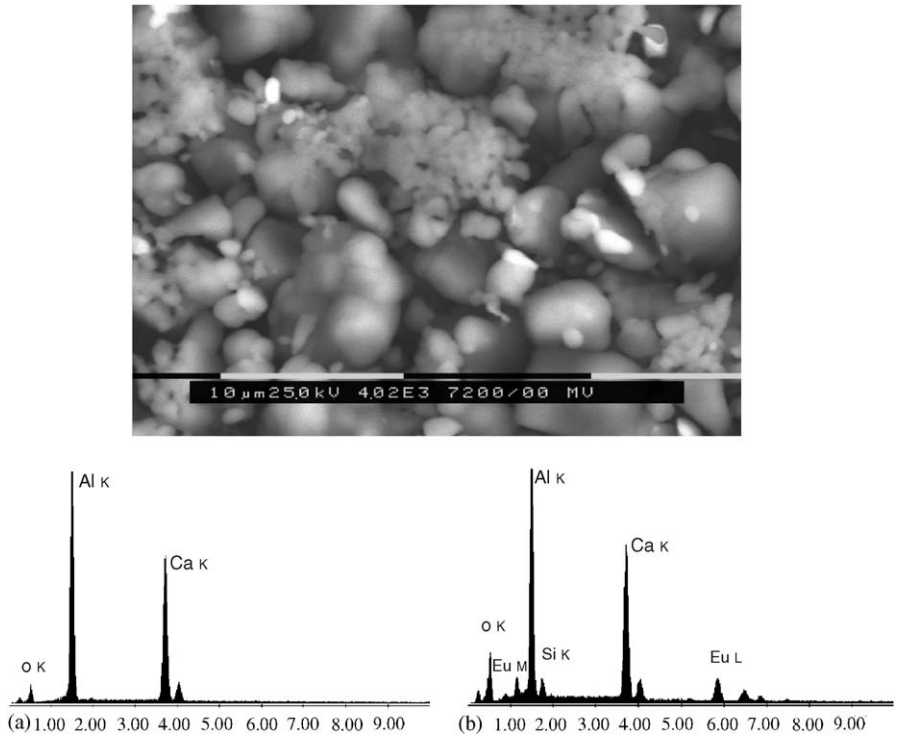

Fig. 4. Backscattered electron image showing the elemental composition of $Ca_{0.99}Al_2O_4:Eu^{3+}$ 1% where the bright regions correspond to the positions of the $CaEuAl_3O_7$ (a) and (b), respectively, are representative EDX spectra of the europium poor and europium rich spectra, respectively.

Table 2
Unit cell parameters for the alkaline earth aluminates and gallates refined from synchrotron X-ray diffraction data

Compound	Space group	a (Å)	b (Å)	c (Å)	β°
$CaAl_2O_4$	$P2_1/n$	8.7024(1)	8.0994(1)	15.2186(2)	90.1651(7)
$SrAl_2O_4$	$P2_1$	8.4394(1)	8.8215(1)	5.15476(9)	93.3965(9)
$BaAl_2O_4$	$P6_3$	10.44854(6)	10.44854(6)	8.78985(6)	—
$CaGa_2O_4$	$Pna2_1$	10.3492(2)	7.7364(1)	9.1274(1)	90
$SrGa_2O_4$	$P2_1/c$	8.3791(1)	8.9965(1)	10.6807(2)	93.9191(8)
$BaGa_2O_4$	$P6_3$	18.6277(1)	18.6277(2)	8.65971(7)	—

It should be noted that for the two barium compounds the standard crystallographic setting was chosen such that γ° is 120°.

Another neutron diffraction pattern was collected at 17 K. At this temperature any paraelectric phase that was trapped in the room temperature sample would, most likely, have equilibrated to form the low-temperature phase removing this from the sample. However the fit to the pattern at this temperature was still poor suggesting the persistence of a high-temperature phase was not the problem.

Examination of the Fourier difference plot suggests the problem may be related to the position of the O(2) anion. This anion connects two tetrahedra that are parallel to each other, and it is most likely that these tetrahedra have some comparative tilting. However, there is still some doubt about the nature of such tilting. Despite this the general structural parameters appear appropriate (Table 3).

The refined structures reveal a number of differences in the environment of the alkaline earth cations. The main difference between the aluminium and gallium cations is that the GaO_4 tetrahedra are more distorted that the AlO_4 tetrahedra. This is most likely caused by the larger size of the Ga^{3+} ion, compared to the Al^{3+} ion, (cf. 0.39 Å for Al^{3+} to 0.47 Å for Ga^{3+} [22]) requiring a distortion to the tetrahedra which form the ring structure in order to accommodate the alkaline earth ions. In all cases, the bond valence sums are within the commonly accepted variation of 10% of expected values of three (see Table 4) [23].

EPR studies have indicated that both Eu^{2+} and the Ln^{3+} co-activators most likely substitute into the alkaline earth ion sites [24–26]. Recent XRD studies by Yamada et al. [27] of a sample of $SrAl_2O_4$ doped with an usually high level of Eu^{2+} have confirmed that the Eu^{2+} occupies the Sr^{2+} sites in $SrAl_2O_4$. It must be noted that in this case the amount of Eu^{2+} doped into the sample is sufficient to change the symmetry of the structure from monoclinic

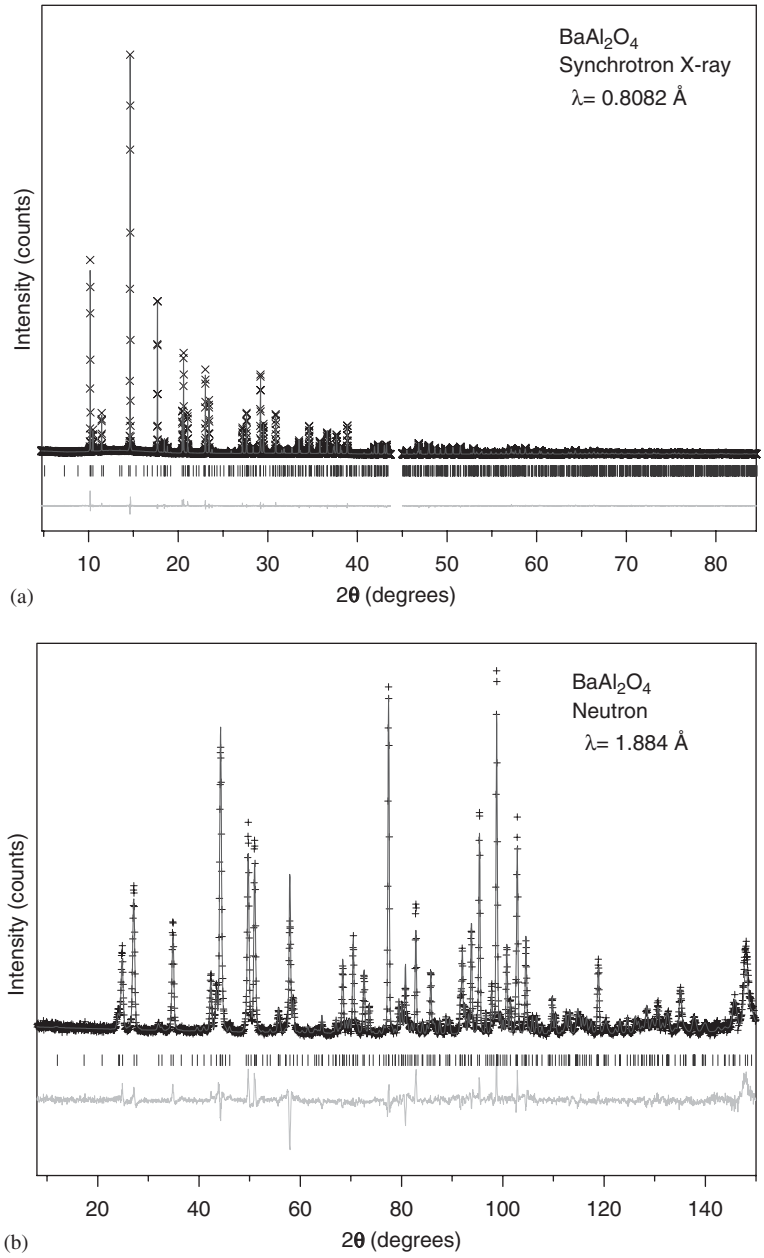

Fig. 5. Refined powder synchrotron X-ray diffraction pattern at room temperature (a) and neutron diffraction pattern at 17 K (b) for $BaAl_2O_4$. The poor fit of the calculated intensity in the neutron diffraction pattern contrasts against the good fit obtained from the synchrotron X-ray diffraction data. The format is the same as for Fig. 2.

Table 3
Statistical measures of fit for the refined models of the alkaline earth aluminates and gallates to their respective neutron and the 5–45° image plate of the synchrotron X-ray data

Compound	Synchrotron X-ray diffraction			Neutron diffraction		
	R_p	R_{wp}	R_B	R_p	R_{wp}	R_B
$CaAl_2O_4$	5.59	7.28	9.36	4.82	5.71	2.07
$SrAl_2O_4$	6.15	8.05	5.33	4.09	4.86	1.5
$BaAl_2O_4$	4.99	6.65	4.24	5.95	7.31	4.44
$CaGa_2O_4$	2.97	3.77	11.27	4.74	5.73	1.61
$SrGa_2O_4$	3.35	4.21	10.04	4.87	5.69	1.97
$BaGa_2O_4$	4.70	6.14	11.01	3.59	4.19	1.99

to hexagonal and this result may not nessecarily apply to alkaline earth aluminate and gallate samples doped with a much smaller amount of Eu^{2+} or Ln^{3+} cations.

The structural details of the alkaline earth aluminates and gallates are of most interest in any attempt to examine the bonding environment likely to be occupied by the lanthanides. The structural details of these compounds can be seen in Tables 4 and 5. The bond valencies calculated for the various alkaline earth sites in the six phases indicate consistent underbonding of these sites. This is most likely a result of the need of the structures to compromise between the more rigid bonding requirements of the tetrahedra, which form the ring structure, and the greater flexibility of

the high co-ordination environment of the alkaline earth ions. This results in the alkaline earth ions occupying sites with longer than optimal A–O bonding distances. This underbonding probably suggests some degree of disorder of either the oxygen anions or the alkaline earth cations as a result of instability in the structure caused by the underbonding of the alkaline earth ions. Attempts to model this disorder particularly in the case of $BaAl_2O_4$, for which the refined structure had a poorer fit to the neutron data, by using split sites proved unsuccessful [27]. A comparison of the aluminate and gallate structures reveals that the underbonding is more significant in the aluminates than it is for the gallates. This underbonding appears to increase with decreasing radii of the alkaline earth ions. This suggests that especially the Ca^{2+} ions are considerably smaller than would be ideal for these structures.

The persistent underbonding of these sites suggests they are unsuitable for the more highly charged Ln^{3+} ions. This is consistent with the segregation of these ions into other phases. The A-type cation sites would have been expected to have bond valencies significantly over two, instead of under two, in order to be able to accommodate appreciable amounts of the more highly charged Ln^{3+} ions. This together with the smaller size of the Ln^{3+} ions, compared to Ba^{2+} and Sr^{2+} ions (cf. ionic radii for Eu^{3+} and Nd^{3+} of 1.12 and 1.16 Å to 1.31 and 1.47 Å for Sr^{2+} and Ba^{2+} [22]) explains the low solubility of Ln^{3+} ions into these sites.

Any Ln^{3+} ions which may be soluble, and there must be some since the Ln^{3+} ions enhance the long-life luminescence properties of these materials, in the host compounds would most likely occupy the alkaline earth sites with the higher effective bond valencies. The extremely low bond valency of the nine co-ordinate site in $CaAl_2O_4$ is a consequence of the unusually long Ca–O bonding distances of this site. This results in a site which is significantly underbonded, despite the larger number of oxygen ions co-ordinated to the Ca^{2+} in this site compared to the other two sites and suggests that, even with the significant distortion from the parent tridymite structure, the Ca^{2+} ion is significantly smaller than would be ideal for this site. The higher bond valencies for the six co-ordinate sites suggests that any Ln^{3+} ions incorporated into the structure are more likely to substitute into these sites as opposed to the nine co-ordinate sites. It is however known that the Eu^{2+} ions prefer the larger nine co-ordinate sites [1]. This would require the europium ions to migrate between the two types of sites during reduction.

The role of bond valence in determining the cation distribution is also illustrated by the impurity phases formed for example $EuCaAl_3O_7$ which forms in $Ca_{0.99}Al_2O_4$:Eu^{3+} 1%. The structure of $EuCaAl_3O_7$ belongs to space group $P\bar{4}2_1m$ and is related to gehlenite, with alternating layers of aluminium tetrahedra and Eu^{3+} and Ca^{2+} ions. The structure refined from synchrotron XRD data showed that Eu^{3+} and Ca^{2+} ions share the same site forming Eu^{3+}–Ca^{2+} pairs which are distributed in a disordered manner [13,14]. The Ca^{2+} and Eu^{3+} ions bond with eight oxygen ions; with six short bonds averaging 2.446(1) Å and two longer bonds averaging 2.862(2) Å. This results in a Eu^{3+} bond valency of 3.00 and a Ca^{2+} bond valency of 1.84. The Al^{3+} ions co-ordinate tetrahedrally with oxygen ions with an average bond length of 1.752(1) and 1.750(2) Å and bond valencies of 3.05 and 3.06 for the two crystallographically distinct sites.

Table 4
Bond valence sums of the alkaline earth, aluminium and gallium sites calculated from the neutron diffraction patterns of these compounds

Compound	$CaAl_2O_4$	$SrAl_2O_4$	$BaAl_2O_4$	$CaGa_2O_4$	$SrGa_2O_4$	$BaGa_2O_4$
A^{2+} 1	1.88	1.69	1.81	2.02	1.94	1.76
A^{2+} 2	1.84	1.83	1.79	1.69	1.78	1.93
A^{2+} 3	1.39	—	—	—	—	1.91
A^{2+} 4	—	—	—	—	—	1.84
A^{2+} 5	—	—	—	—	—	1.80
A^{2+} 6	—	—	—	—	—	1.76
B^{3+} 1	3.07	3.12	3.21	2.89	2.98	2.81
B^{3+} 2	3.00	2.96	2.99	3.00	2.98	2.89
B^{3+} 3	2.94	3.02	2.96	2.87	2.88	2.98
B^{3+} 4	2.99	3.06	2.97	2.87	2.95	3.10
B^{3+} 5	2.98	—	—	—	—	3.02
B^{3+} 6	3.04	—	—	—	—	3.14
B^{3+} 7	—	—	—	—	—	2.94
B^{3+} 8	—	—	—	—	—	3.06

A^{2+} corresponds to the alkaline earth ion present in each compound while B^{3+} corresponds to Al^{3+} and Ga^{3+} for the aluminates and gallates respectively and the number refers to the atomic sites.

Table 5
Average bond lengths (Å) and number of bonds of the A^{2+} sites in the alkaline earth aluminates and gallates

Crystallographic site	A^{2+} 1	A^{2+} 2	A^{2+} 3	A^{2+} 4	A^{2+} 5	A^{2+} 6
$CaAl_2O_4$	6 × 2.409(4)	6 × 2.429(4)	9 × 2.781(3)	—	—	—
$SrAl_2O_4$	6 × 2.622(3)	6 × 2.606(2)	—	—	—	—
	3 × 3.371(5)	4 × 3.490(9)				
$BaAl_2O_4$	9 × 2.89(1)	9 × 2.91(1)	—	—	—	—
$CaGa_2O_4$	6 × 2.431(3)	6 × 2.472(4)	—	—	—	—
	2 × 3.023(6)	2 × 3.291(6)				
$SrGa_2O_4$	6 × 2.572(3)	6 × 2.688(3)	—	—	—	—
	2 × 3.201(5)	3 × 3.556(4)				
$BaGa_2O_4$	9 × 2.95(1)	7 × 2.83(1)	8 × 3.01(1)	9 × 2.932(9)	9 × 2.931(9)	7 × 2.845(9)

$ALnM_3O_7$ compounds have been systematically studied previously [13] and it is known that the relative size of the cations significantly affects the stability of each phase. $BaLnAl_3O_7$ compounds do not form due to the mismatch in the size of the Ba^{2+} and Al^{3+} ions [13] and while $SrLnAl_3O_7$ compounds are known to form, it appears that the mismatch in the size of strontium and the aluminium ions is large enough so that the alternative $LnAlO_3$ phases are more stable. Hence these form in Eu^{3+} and Nd^{3+} doped strontium and barium aluminate. For lanthanides smaller than samarium, $BaLnGa_3O_7$ type phases do not form, [13] hence explaining why $BaEuGa_3O_7$ does not form.

Likewise analysis of synchrotron XRD data for $EuAlO_3$ demonstrates the importance of bond valencies in determining which phases form. The europium site has an average bond distance of 2.472(3) Å, for the eight nearest neighbouring oxygen ions and 3.027(4) Å for the next four nearest neighbouring oxygen ions resulting in a bond valency for the europium site of 3.19 much higher than the bond valencies for the alkaline earth aluminates. The Al^{3+} ions have an average bonding distance of 1.903(3) Å and a bond valency of 3.04.

The elimination of the europium segregation in the reduced samples can be interpreted as Eu^{3+} reducing to Eu^{2+} which is then incorporated into the host. This is a result of the Eu^{2+} ions, which have a lower charge to size ratio, being better suited to the A^{2+} sites with their bond valencies of approximately two, than is the case for the Ln^{3+} co-activating ions. This is supported by electronic spectra which feature an intense broad peak centred at 315–325 nm which can be assigned to the $4f^7 \rightarrow 4f^6 5d^1$ transition of Eu^{2+} confirming that Eu^{3+} does indeed reduce to form Eu^{2+} [28]. Interestingly the rate of the Eu^{3+} reduction appears to increase as ionic radius of the A^{2+} ions, it is substituting for, increases. This is chemically sensible as the larger the site in the alkaline earth aluminate the more readily the large Eu^{2+} cation will fit. The size difference between Ca^{2+} and Eu^{2+} (cf. 1.18 Å for Ca^{2+} and 1.30 Å for Eu^{2+} [22]) suggests that substitution of Eu^{2+} ions, even into the larger Ca^{2+} nine co-ordinate site, requires significant distortion to the structure of the host. This would require significantly more energy than for the substitution of Eu^{2+} into strontium and barium aluminate (cf. 1.31, 1.47 and 1.30 Å for Ba^{2+}, Sr^{2+} and Eu^{2+}, respectively [22]), where any structural distortion would be far smaller. This results in the slower rate of incorporation, and therefore reduction, for europium into the calcium aluminate sample.

5. Conclusion

The aim of this work was to establish the likely fate of the rare-earth cations when they are added to the stuffed tridymite AM_2O_4 ($A^{2+} = Ca^{2+}$, Sr^{2+} and Ba^{2+}, $B^{3+} = Al^{3+}$ and Ga^{3+}). Using a combination of synchrotron X-ray and neutron powder diffraction accurate and precise structures for the six oxides have been obtained. Bond valence analysis shows the local bonding of the *B*-type cations, located at the centre of the BO_4 tetrahedra, to be unexceptional. Conversely the bonding environments of the larger *A*-type cations, that occupy a number of sites within the channels formed by the corner sharing BO_4 tetrahedra, vary considerably. In all cases underbonding of the *A*-type cations is evident, this being most apparent for the smaller *A*-type cations (calcium and to a lesser extent strontium).

When these oxides are doped with rare-earth cations we observe partial segregation of these dopants. It is thought that this is a consequence of the less than optimal fit of the trivalent rare-earth cations into the *A*-type sites of the stuffed tridymite structure. When the rare-earth is europium reduction to Eu^{2+} increases the solubility of the cation into the host. The inability to encapsulate significant amount of trivalent lanthanide cations in these structures is of potential importance in the optimisation of these for use in luminescent materials.

Acknowledgments

The authors would like to thank AINSE for access to the HRPD instrument used for neutron diffraction measurements and the ASRP for access to the ANBF used to collect the synchrotron diffraction data. We would also like to thank Dr. James Hester for his assistance with collecting the data at the ANBF.

Appendix A. Supplementary materials

Supplementary data associated with this article can be found in the on-line version at doi:10.1016/j.jssc.2005.10.043.

Reference

[1] T. Aitasalo, P. Deren, J. Hölsä, H. Junger, J.-C. Krupa, M. Lastusaari, J. Legendziewicz, J. Niitykoski, W. Strek, J. Solid State Chem. 171 (2003) 114–122.
[2] T. Matsuzawa, Y. Aoki, N. Takeuchi, Y. Murayama, J. Electrochem. Soc. 143 (1996) 2670–2673.
[3] A.H. Kitai, T. Xiao, SID 97 Digest 28 (1997) 419–422.
[4] V. Kahlenberg, R.X. Fischer, J.B. Parise, J. Solid State Chem. 154 (2000) 612–618.
[5] V. Kahlenberg, R.X. Fischer, C.S.J. Shaw, J. Solid State Chem. 153 (2000) 294–300.
[6] S.-Y. Huang, R. von der Muehll, J. Ravez, M. Couzi, Ferroelectrics 159 (1994) 127–132.
[7] S.-Y. Huang, R. von der Muehll, J. Ravez, M. Couzi, J. Solid State Chem. 110 (1994) 97–105.
[8] H. Müeller-Buschbaum, A.R. Schulze, Z. Anorg. Allg. Chem. 475 (1981) 205–210.
[9] A.R. Shulze, H. Müeller-Buschbaum, Z. Anorg. Allg. Chem. 475 (1981) 205–210.
[10] W. Hörkner, H. Müller-Buschbaum, J. Inorg. Nucl. Chem. 38 (1976) 983–984.
[11] H.-J. Deiseroth, H. Müeller-Buschbaum, Z. Anorg. Allg. Chem. 396 (1973) 157–164.

[12] H.-J. Deiseroth, H. Müeller-Buschbaum, Z. Anorg. Allg. Chem. 402 (1973) 201–205.
[13] J.M.S. Skakle, R. Herd, Powder Diffr. 14 (1999) 195–202.
[14] Y.E. Smirnov, I.A. Zvereva, R.A. Zvinchuk, Russ. J. Gen. Chem. 72 (2002) 1848–1852.
[15] Y. Kanke, A. Navrotsky, J. Solid State Chem. 141 (1998) 424–436.
[16] T.M. Sabine, B.J. Kennedy, R.F. Garrett, G.J. Foran, D.J. Cookson, J. Appl. Crystallogr. 28 (1995) 513–517.
[17] C.J. Howard, C.J. Ball, R.L. Davis, M.M. Elcombe, Aust. J. Phys. 36 (1983) 507–518.
[18] B.A. Hunter, C.J. Howard, Rietica for windows, 1.7.7, Sydney, 1997.
[19] A.M. Abakumov, O.I. Lebedev, L. Nistor, G. Van Tendeloo, S. Amelinckx, Phase Transitions 71 (2000) 143–160.
[20] S. Ito, K. Suzuki, S. Naka, Mater. Res. Bull. 15 (1980) 925–932.
[21] D.C. Do, C. Bertatu, Bull. Soc. Frans. Miner. Cristallogr. 88 (1965) 413–416.
[22] R.D. Shannon, Acta Crystallogr. A 32 (1976) 751–767.
[23] I.D. Brown, D. Altermatt, Acta Crystallogr. B 41 (1985) 244–247.
[24] T. Nakamura, K. Kaiya, N. Takahashi, T. Matsuzawa, M. Ohta, C.C. Rowlands, G.M. Smith, P.C. Riedi, Phys. Chem. Chem. Phys. 3 (2001) 1721–1723.
[25] T. Nakamura, K. Kaiya, N. Takahashi, T. Matsuzawa, C.C. Rowlands, V. Beltrán-López, G.M. Smith, P.C. Riedi, Phys. Chem. Chem. Phys. 1 (1999) 4011–4014.
[26] T. Nakamura, K. Kaiya, N. Takahashi, T. Matsuzawa, C.C. Rowlands, V. Beltrán-López, G.M. Smith, P.C. Riedi, J. Mater. Chem. 10 (2000) 2566–2569.
[27] H. Yamada, W.S. Shi, C.N. Xu, J. Appl. Crystallogr. 37 (2004) 698–702.
[28] S.H.M. Poort, W.P. Blokpoel, G. Blasse, Chem. Mater. 7 (1995) 1547–1551.